ONE-DIMENSIONAL DYNAMIC MODEL OF A PAPER FORMING PROCESS

Paul F. Turnbull
Graduate Research Asst.
University of Michigan
Ann Arbor, MI 48109

William W. Schultz
Associate Professor
University of Michigan
Ann Arbor, MI 48109

Noel C. Perkins
Associate Professor
University of Michigan
Ann Arbor, MI 48109

Paul D. Beuther
Associate Research Fellow
Kimberly-Clark Corp.
Neenah, WI 54956

ABSTRACT

A one dimensional, unsteady model of the wet end of a paper forming process is derived from fundamental conservation laws. The stock is approximated as an inviscid fluid and the wire as an axially moving medium subjected to a fluid loading. Forming lengths are reasonable predicted when compared to test data. Despite heavy damping, the model shows significant amplification of disturbances near resonant frequencies resulting in significant machine-direction (MD) basis weight variations.

INTRODUCTION

This study focuses on the mechanics of the wet forming region of a paper process. The motivation for the study is to gain an understanding of the formation of tissue in a *crescent* forming machine. The crescent forming process involves a water/fiber fluid *stock* sprayed as a jet at a porous *wire* screen. The wire allows the water to pass through but traps the fibers. The wire, forming a wide continuous and translating belt, wraps around a large roll, called the *form roll*. Only one-sided drainage is considered here. The forming region, illustrated in Figure 1, extends from the point where the fluid jet impinges on the wire to the point where the fibrous mat touches the roll.

Previous theoretical models of paper forming focus on overall measures of the forming process and do not provide either detailed or comprehensive descriptions of mat formation. An early theoretical study of the forming region by Miller [1] sought to estimate the overall drainage rate through the mat and wire. A later study [2] made improvements in the drainage estimate specifically for a *Fourdrinier* machine that passes a wire horizontally over a series of small rollers during the drainage process. Using an assumption of symmetry, Baines [3] examined the mechanics of a two-wire machine that permits water to pass through an inner wire and porous roll as well as an outer wire. However, the assumed symmetry in the forming region is inconsistent with the inclusion of centrifugal terms in the pressure equation. (Modifications of the model presented here for the two-wire machine are briefly described in Turnbull [4].) To date, all models of the forming region assume that the forming process is steady-state. Direct observations of wire vibration and variations in mat thickness (variations in *basis weight*), however, indicate that the forming process is often unsteady including recent experiments such as Perrault [5].

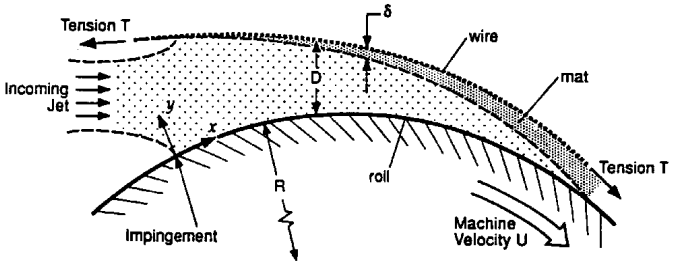

Figure 1: Schematic of the forming region

The wire falls within a broader class of dynamical systems commonly referred to as *axially moving materials* [6]. Examples of other axially moving materials include: band saw blades, translating cables, belts and tapes. Recent developments in the vibration and stability of axially moving material systems are reviewed by Wickert and Mote [7]. Wire vibration leads to dynamic contact between the wire and roll that changes the length of the vibrating span and may affect the wire response [8, 9]. The present investigation also relates to studies of the response of web-like elements in a surrounding fluid [10, 11]. In such studies, the fluid response on the web is modeled using "added mass" coefficients, originally derived in the context of the swimming of a slender fish approximated as an impermeable, flexible structure in an infinite fluid medium [12]. The present application demands an alternative approach for modeling the fluid/structure interaction because it violates the assumptions of structure impermeability and infinite fluid medium.

The next section describes the mathematical model used to predict the mechanics of a paper forming process. The numerical implementation is then detailed followed by the resulting predictions. The conclusions drawn from the results highlight how the coupled fluid/wire dynamics influence product quality.

THE MODEL

Direct observations of wire vibration in the forming region and non-uniform mat thickness indicate that the forming process is often unsteady. This time dependent response may be driven by several excitation mechanisms. Foremost among these are time dependent jet velocity perturbations from the jet delivery system that may derive from the pump, headbox, etc. Secondary excitation sources include fluid turbulence, roll eccentricity, periodic passage of

wire splices and mechanical perturbations originating from operations outside the forming region. In view of the slender geometry of the forming region, these seemingly small excitation sources have the potential to generate process-impairing wire vibrations.

Figure 1 defines the problem of interest and the model coordinate system. The (x, y) coordinate system is curvilinear and locally Cartesian with the arc length along the roll defining x and position along the direction normal to the roll defining y. The origin of the coordinate system is at the fluid impingement point with the roll that is assumed to be stationary. We further assume no variation in the third direction (the cross machine direction). $D(x,t)$ denotes the gap between the wire and the form roll, the mat thickness is $\delta(x,t)$ and the fluid velocity component in the x direction is $u(x,t)$. The form roll and the wire move with machine speed U and the wire has tension T (force per unit width).

The fluid entering the domain has density ρ, viscosity μ, and a volumetric concentration of fibers C_f. The Reynolds number $\rho U D(x=0)/\mu$ is large, implying that the boundary layer along the roll will be thin and viscous effects in the fluid will be confined to a small region near the end of the forming region. Thus, the fluid velocity can be assumed to be rectilinear and an inviscid model is attempted. These assumptions lead to a one-dimensional model where x is the single independent spatial coordinate along with the time variable t.

The problem domain begins at a point shortly after the fluid impinges on the wire and roll where the fully three dimensional flow of the entrance region has collapsed to a one dimensional flow. This transition occurs almost immediately after both the wire and roll are wetted as is shown in the section entitled "Steady-state Response". The problem domain extends to a fixed position beyond the point where the mat is always in contact with the roll. The domain effectively splits into two subdomains: a fluid-dominated subdomain upstream of the contact point where the mat first touches the roll $x < \hat{x}$, and a structure-dominated subdomain downstream of the contact point $x > \hat{x}$. The location of the contact point, $\hat{x}$, is not known *a priori* and is found via the solution procedure. The primary difference between these two subdomains is the origin of the force supporting the wire. In the fluid-dominated subdomain the force originates from the fluid pressure and in the structure-dominated subdomain the force is supplied by the contact of the fibers in the mat. In the present formulation, the two subdomains are joined by means of a function which smoothly blends the governing equations for each subdomain together over a small region near the contact point $\hat{x}$. In this small region, viscous forces become non-negligible and thus neither subdomain model is strictly appropriate. However, since mat formation is virtually complete before the transition between subdomains, the behavior of the model is found to be insensitive to changes in the modeling of the downstream end.

In addition to assuming inviscid flow, the principal modeling assumptions include: 1) the fluid impingement point is stationary, 2) there is no variation in the cross machine direction, 3) the wire vibrations are small so that the wire tension T is assumed constant and the wire curvature-displacement relation is linear, 4) the fluid velocity is rectilinear, 5) the void fraction of the mat ϵ is constant and 6) the mass of the wire per unit area (including the mat and entrained water) is constant. Of these, assumption 6) is easiest to relax, but for simplicity, we choose the average mass of the mat and wire to represent the mass for the entire length of the forming region. Relaxation of assumption 5) requires only a more elaborate model for the flow through the porous media. Relaxation of 2) results in a two-dimensional extension of the present model and is the subject a subsequent study. Given these assumptions, the governing equations derived below from the fundamental conservation laws are exact.

Conservation of water in one-dimension is given by

$$\begin{aligned}(1-C_f)\,(D-\delta)_t + \epsilon\delta_t = \\ -\left[(1-C_f)u(D-\delta) + \epsilon U\delta\right]_x - v.\end{aligned} \tag{1}$$

Here, C_f is the volumetric fiber concentration in the fluid and v is the apparent fluid velocity normal to the wire, the so-called *drainage velocity*. The subscripts t and x denote partial differentiation with respect to these variables. The terms on the left-hand side account for the accumulation of water between the mat and the roll and in the mat. These terms are balanced by the difference between the change in the volume flow rate and the drainage velocity.

Conservation of fiber mass provides

$$C_m\delta_t + C_f\,(D-\delta)_t = -C_m U\delta_x - C_f\left[u\,(D-\delta)\right]_x, \tag{2}$$

where C_m is the volumetric fiber concentration in the mat (note that $C_m = 1-\epsilon$). Here, the left-hand side represents the accumulation of fibers in the mat and in the fluid between the mat and roll. The accumulation is due to the change in the x direction of fibers being convected downstream in the mat and the fluid, respectively. This expression for conservation of fibers can be simplified to

$$\delta_t + U\delta_x = -\frac{C_f}{C_m}\{(D-\delta)_t + [u(D-\delta)]_x\}. \tag{3}$$

Neglecting fluid viscosity except in the mat, conservation

of momentum yields the unsteady Euler equation

$$u_t + uu_x = -\frac{1}{\rho}p_x, \tag{4}$$

stating that the change of the fluid momentum along the machine direction is determined by the pressure gradient. The transverse response of the wire is governed by

$$D_{tt}+2UD_{xt}+U^2D_{xx}-\frac{U^2}{R} = \frac{T}{m}\left(D_{xx} - \frac{1}{R} + \frac{p}{T}\right), \tag{5}$$

where m (approximated as a constant) is the mass of the wire, the mat, and the entrained water per unit area. R is the form roll radius as shown in Figure 1. The terms on the left-hand side represent the absolute acceleration of a wire element including the convective acceleration components due to wire translation around the form roll [6]. Additionally, the term $T/m(1/R)$ on the right-hand side results from the curvature of the coordinate system. The quantity p on the right-hand side of (5) represents the force per unit area exerted by the fluid or mat on the wire. Thus, in the fluid-dominated subdomain, $x < \hat{x}$, p is the fluid pressure determined by the resistance of the flow through the mat using the empirical relation

$$p = a(\delta + \delta_w)v + b(\delta + \delta_w)v^2, \tag{6}$$

where $a = \mu/\kappa$ and $b = C_e\rho/\sqrt{\kappa}$. Here κ is the permeability of the mat and wire (as determined by the fiber diameter and void fraction [13]), μ is the viscosity of water, ρ is the density of water and C_e is the Ergun coefficient that is adjusted to fit experimental data as described in the section entitled "Steady-state Response." In (6) δ_w represents the resistance to flow through the wire expressed as an equivalent mat thickness. In this study, δ_w is chosen 10^{-5} m and for 20 micron fibers with a void fraction of 90% $2153\frac{\text{kg}}{\text{m}^3\text{s}}$. The term proportional to v^2 accounts for the inertial effects present in a thin porous media. In the limit of vanishing b, this expression becomes a one-dimensional integrated form of Darcy's law for flow through porous media. Note that the pressure p provides the coupling between the fluid and the wire. Since the pressure is proportional to v and v^2, which in turn are related to D_t (1), the pressure may be interpreted as a nonlinear damping mechanism for wire vibration. The affect of this damping is discussed in the section entitled "Unsteady Response."

The structure-dominated subdomain is described by the translating wire supported by a compressible mat modeled as an elastic foundation. Previous analysis of translating elements on elastic foundations are described in Bhat [14], Perkins [15] and Tan [16]. In this subdomain, the wire response is again governed by (6) where now p is the force per unit area created by an elastic foundation

$$p = k(F - D). \tag{7}$$

Here, k is an effective mat stiffness per unit area and F is a constant representing the free height of a theoretical distributed spring that balances the tension in the wire. These two constants are chosen such that the spring force p balances the tension T at the downstream boundary and the spring remains in compression for the full length of the structural domain. At steady-state, p approaches T/R as D approaches δ. Computed results have been shown to be insensitive to changes in k and F and in the modeling of the boundary between the fluid-dominated and structure-dominated subdomains. This insensitivity is due to the dominance of the fluid-dominated subdomain and the bias in the flow of energy downstream (in the machine direction). Thus, changes at this downstream boundary exert little influence on the forming process occurring upstream.

The above dependent variables now are made dimensionless by employing the length scale defined by the form roll radius R, the time scale R/U, and a pressure scale T/R. Equations (3), (4) and (5) define a system of three partial differential equations that are fourth order in time and fifth order in space. The equations are

$$\delta_t + \delta_x = -\frac{C_f}{C_m}\left[(D-\delta)_t + (u\,(D-\delta))_x\right], \tag{8}$$

$$u_t = -\frac{T}{\rho R U^2}p_x - uu_x, \tag{9}$$

$$D_{tt} + 2D_{xt} + D_{xx} - 1 = \frac{T}{mU^2}\left(D_{xx} - 1 + p\right). \tag{10}$$

The system of equations is completed by solving for v in (1) resulting in

$$v = -(1-C_f)\left[(D-\delta)_t + (u(D-\delta))_x\right] + \epsilon(\delta_t+\delta_x) \tag{11}$$

and then substituting the result into (6) and forming an algebraic expression for p

$$p = \frac{R^2U}{T}(\delta + \delta_w)(av + bUv^2). \tag{12}$$

The associated boundary conditions are

$$D(0,t) = D_0, \quad D(L,t) = D_L, \tag{13a,b}$$

$$\delta(0,t) = 0, \qquad u(0,t) = U_0, \tag{13c,d}$$

$$p(0,t) = P_0. \tag{13e}$$

These boundary conditions may be time-dependent to allow for possible excitation mechanisms including, jet velocity fluctuations and roll eccentricity. Motion may also follow from initial conditions of the form

$$D(x,0) = f(x), \qquad D_t(x,0) = g(x), \tag{14a,b}$$

$$\delta(x,0) = q(x), \qquad u(x,0) = r(x). \tag{14c,d}$$

The above initial conditions also determine the initial drainage velocity $v(x,0)$ and the initial pressure profile $p(x,0)$ through (11) and (12).

NUMERICAL ANALYSIS

This model couples a parabolic fluid advection equation (9), a hyperbolic wave propagation equation (10) and the equations governing the conservation of mass of an incompressible fluid/fiber stock (8) and (12). Taken separately, these different types of equations require qualitatively different solution strategies. Also, there are complexities due to the two subdomains needed to model the unknown location of the contact point. The numerical strategy must overcome a unique set of difficulties.

The fluid advection equation (9) is solved using an upwind technique employing explicit, Adams-Bashforth time integration [17]. This method preserves the bias in the flow of information in the downstream direction and provides a method that is conditionally stable for sufficiently small time steps. The mat evolution equation (8) and fluid conservation equation governing the pressure (12) have less bias in the flow of information. Central-difference in space and Adams-Bashforth explicit time integration was found to be conditionally stable. The fluid velocity and mat thickness are advected downstream in the structural subdomain using a first order upwind method.

The wave equation (10), governing the vibration of the wire, is also discretized using central-difference approximations and integrated in time using a Crank-Nicolsen implicit method. Normally this scheme is unconditionally stable for arbitrary time steps. However, due to the interaction with the fluid, the discretized version of (10) loses its unconditional stability. The scheme is rendered conditionally stable for sufficiently small time steps. For example, the maximum stable time steps for three different non-dimensional grid sizes are shown in Table 1.

Table 1: Maximum stable time step versus grid size

Grid size	Time step
0.011	0.0017
0.0054	0.00045
0.0027	0.00014

The location of the contact point and thus the length of the forming region is unknown and must be found as part of the solution of the system of equations. To accomplish this, the computational domain is split into two sub-domains as described previously. The two subdomains are blended into a single continuous computational domain by means a function s defined as

$$s = \frac{1}{2}\left[\tanh\left(c_1\frac{\delta}{D} - c_2\right) + 1\right], \tag{15}$$

where $0 < s < 1$. The equations governing the fluid-dominated subdomain are multiplied by $(1-s)$ and those governing the structure-dominated subdomain are multiplied by s and these product equations are added. The constants c_1 and c_2 are chosen such that $s \ll 1$ over most of the forming region and then smoothly approaches $s \to 1$ when $\delta/D \to 1$. Figure 2 illustrates a typical shape of the blending function for $c_1 = 6$ and $c_2 = 3$.

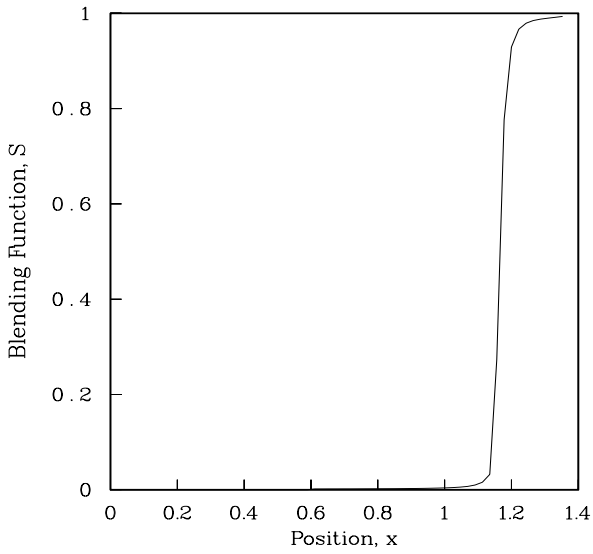

Figure 2: An example of the function $s(x)$ used to blend the fluid dominated and structure dominated subdomains.

The values chosen for the boundary conditions are adjusted to simulate specific paper making machines. The initial gap between the wire and roll D_0 is chosen to be equal to the height of the jet. The downstream boundary condition D_L is set to the theoretical steady-state mat thickness based on global fiber conservation,

$$D_L = \frac{C_f U_0 D_0}{C_m U}. \tag{16}$$

The jet velocity U_0 is usually chosen to be equal to the machine speed. However, it can be set lower or higher to examine the effects of a velocity differential between the fluid and the wire. Such a velocity differential is typically

Table 2: Parameters defining the baseline system

Parameter	Value	units
Slice height D_0	12.7	mm
Downstream height D_L	0.168	mm
Upstream pressure P_0	9000	Pa
Form roll radius	0.56	meters
Machine speed	25.4	m/s
Wire tension	7881	N/m
Wire mass	1.0	kg/m^2
Headbox consistency C_f	0.132	%
Void fraction ϵ	0.9	
Jet/Machine speed ratio	1.0	

desirable due to its influence on fiber orientation and the resulting influence on mat tensile strength.

The pressure at the beginning of the one-dimensional region P_0, however, is not as easily determined due to higher dimensional entrance effects (ie. transition from free jet to a confined fluid layer). The pressure after these entrance effects is not known a priori, nor can the pressure measured at the *roll* be used to determine the pressure at the *wire* at the jet impingement. Instead, the pressure P_0 is chosen to avoid substantial oscillations of the pressure profile. This is accomplished by iterating on P_0 until the quantity $\frac{\partial^2 P(0,t)}{\partial x^2} = 0$. The method starts with the initial guess for the upstream pressure as $P_0 = T/2R$ and a simulation is run to steady-state. If $\frac{\partial^2 P(0,t)}{\partial x^2} < 0$ at steady-state, the value for P_0 is considered to be too small. Similarly, P_0 is too large if this second derivative is positive. The upstream pressure is subsequently adjusted until a smooth pressure profile is obtained. Then P_0 is held constant during the subsequent simulations of unsteady response.

NUMERICAL RESULTS

The above numerical method is used to examine both the steady-state and unsteady response of a paper forming process. We first consider the simpler steady-state case.

Steady-state Response

A baseline system is proposed for study as defined by the parameters shown in Table 2. Unless otherwise noted, all computed results that follow pertain to this baseline system. The mesh size chosen for all the steady-state computations to follow is 0.011. Increasing the number of nodes does not appreciably alter the steady-state results and we conclude that the following results are well converged.

In the absence of excitation, a stable system is expected to settle to a stable steady-state following any perturbation (e.g., initial conditions). Determining the steady-state solution for a particular set of system parameters makes it possible to calibrate the adjustable parameter b (by adjusting the Ergun coefficient C_e) in the fluid resistance relation (12). This is accomplished by comparing computed results for the forming length to that measured on a forming machine operating with the same set of system parameters and adjusting b such that the forming lengths match. Alternatively, all three parameters in the fluid resistance relation (12) δ_w, a and b may be adjusted to produce a better fit of the forming length for broader operating conditions.

Major capabilities of the steady-state model include the ability to predict the forming region geometry, the drainage profile and the pressure profile. An example of the predicted steady-state pressure profile is illustrated together with experimental measurements in Figure 3. From this

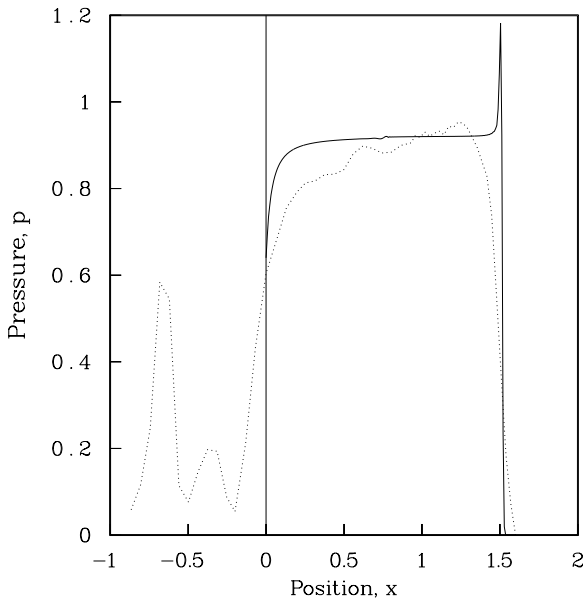

Figure 3: The pressure profile as measured on a crescent former (· · · · · ·) and as calculated by the model (————) for the baseline system. Pressure p is scaled by T/R and position x is scaled by R. This type of comparison is used to calibrate the resistance parameter b in (12).

comparison, the adjustable parameter b was selected by setting $C_e = 14$ to match this test data and all subsequent results use this value.

Examination of the test data reveals an initial pressure spike occurring at the impingement of the fluid on the roll followed by a region of low pressure. At $x = -0.2$ both the wire and roll become wetted and the pressure rises monotonically. After a short entrance region $-0.2 < x < 0$ the fluid mechanics have collapsed from the fully three dimensional flow of the jet to the one dimensional flow of the trapped fluid layer. From this point, defined as $x = 0$, the assumptions of the model are valid and the computational domain begins. Note that the predicted pressure is asymptotic to a value near T/R which produces a wire geometry with very little curvature relative to the roll. Thus, the gap D between the wire and the roll decreases almost linearly with the arc length coordinate x. This nearly linear geom-

etry occurs despite the very non-uniform drainage velocity v as shown in Figure 4. The final mat thickness was found to be 1% less than the theoretical value given by global conservation of fibers (16).

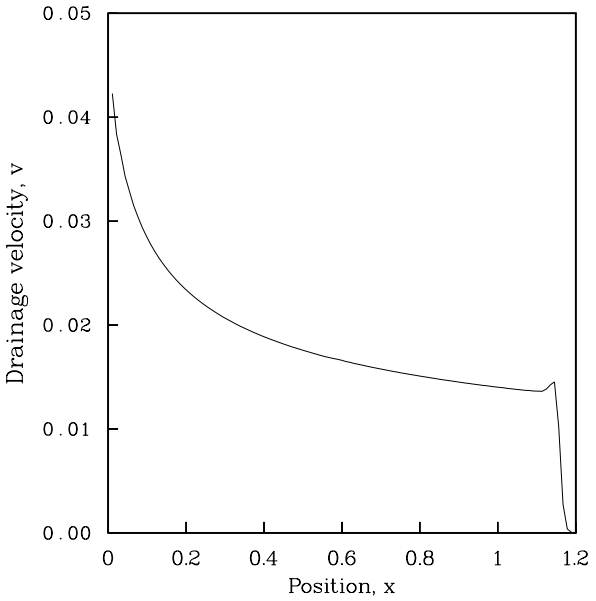

Figure 4: The steady state drainage velocity v as a function of x for the baseline system. Drainage velocity v is scaled by U and position x is scaled by R.

The model is capable of predicting the steady-state geometry of the forming region for a range of parameters near those used to calibrate the parameter b. For example, the variation in forming length with respect to the fiber concentration in the stock, C_f (known as the *headbox consistency*) is shown in Figure 5. Similarly, the variation in forming length with respect to tension is shown in Figure 6. Both show smooth monotonic behavior over the range of parameters modeled and, as expected, the forming length increases with increasing headbox consistency and decreases with increasing tension.

Unsteady Response

The time dependent model computes the system response under both free and forced conditions. For free response, the system is perturbed by selected initial conditions and the ensuing transient response is computed. For forced response, the system is perturbed by unsteady upstream boundary conditions. For all computations to follow, the response of selected quantities (e.g., wire displacement and fluid velocity) are sampled at the mid point of the fluid-dominated subdomain (a single node value) unless otherwise noted.

Consider first, the free response of the wire, as measured by the mid-point displacement D_{mid} above the roll as shown in Figure 7. This response is normalized by the steady-

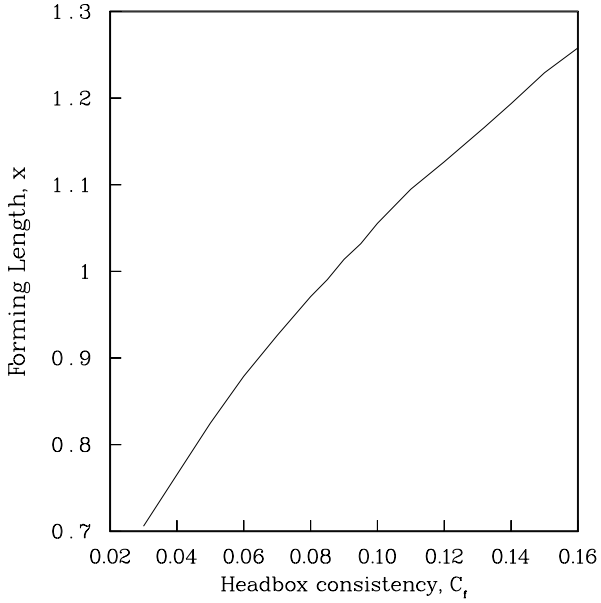

Figure 5: The steady state forming length $\hat{x}$ (scaled by R) as a function of the headbox consistency C_f.

state displacement D_{ss}. The system is started from steady-state and given an initial transverse velocity with a maximum amplitude $D_t = 0.01$ at the mid-point of the fluid dominated sub-domain and a half sine wave shape in x. From Figure 7, it is apparent that there is a short period growing of transient response followed by a rapid relaxation to steady-state. This short transient is evidence of the substantial damping inherent in the momentum equation for the wire. This damping is due to the energy lost as the fluid is forced through the porous media through the resistance relation for the flow through the mat and wire in (12). From the oscillations evident in the free response, it is also possible to estimate the natural frequency of the fundamental mode of the system, that has a period of approximately one time unit (non-dimensional). Such oscillations lead to disturbances with a wavelength of approximately one roll radius.

Next consider the forced response of the system to a small harmonic variation in the inlet jet velocity given by $u(0,t) = u_0(1 + A\cos\omega t)$. Here, u_0 is the steady component of the jet velocity (set equal to 1 in this example), A and ω are the amplitude and frequency of the dynamic component of the jet velocity. In this calculation the forcing is held constant at $A = 0.01$ while the excitation frequency ω is varied over the range $0 < \omega < 6$. For each value of ω the system is integrated until it reaches a steadstate oscillation. The amplitude of the variation in D, δ and u are then reported in the frequency response results of Figures 8, 9 and 10 respectively. In contrast to the steady-state computations, the grid resolution modestly influences the magnitude of the results. Results are shown for two grid sizes, $\Delta x = 0.011$, and $\Delta x = 0.0054$, illustrating the small difference in response amplitude with increasing grid

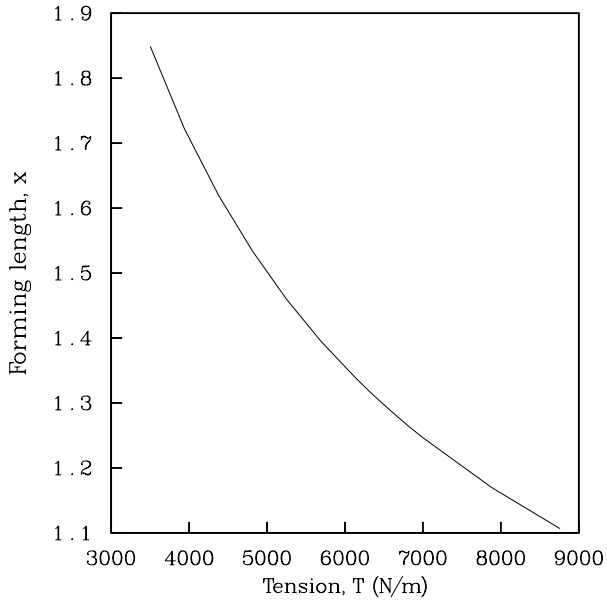

Figure 6: The steady state forming length $\hat{x}$ (scaled by R) as a function of the wire tension T expressed in dimensional units (N/m).

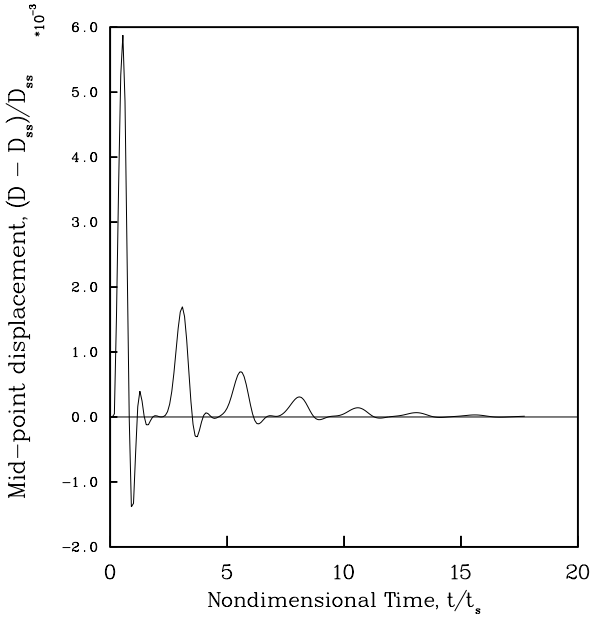

Figure 7: Transient wire response represented by the motion of the midpoint ($x = L/2$) of the wire normalized by the steady state displacement of the wire at the midpoint. Time is made dimensionless using the time scale, $t_s = R/U$.

refinement. Temporal convergence is assured by selecting a time step an order of magnitude smaller than the time step required for stability at the spatial resolutions indicated.

Figure 8 shows the normalized peak mid-point displacement of the wire D_{peak} as a function of the excitation frequency. The frequency response of the wire shows a single broad peak indicative of a single degree-of-freedom, heavily damped system. Although the wire has infinite degrees of freedom, the response of the higher frequency modes are suppressed by damping. This is shown by the absence of higher order peaks in the wire frequency response shown in Figure 8. The resonant behavior of the wire has a pronounced influence on the basis weight of the final product (computed from the mat thickness at the end of the forming region $\delta(L,t)$) as shown in Figure 9. As was the case with the wire response, there is substantial disturbance amplification evident in the response of the basis weight. Moreover the disturbance wavelength is again, approximately one roll radius. The frequency response of the peak fluid velocity however, has a local minimum (anti-resonance) near the frequency corresponding to the peak wire response as shown in Figure 10. This is explained below by examining the phase relationship between the response of the wire and the response of the fluid.

Figure 11 shows the phase relationship between the wire and fluid responses in the vicinity of the local minimum in the peak fluid velocity. The phase was computed by comparing the time when the peak in the fluid velocity occurs versus the time when the peak displacement of the wire occurs. Note that the drop in the peak fluid velocity occurs when the fluid response is in phase with the wire response. This is expected from conservation of mass. If the displacement of the wire is increasing as the fluid velocity is increasing then there will be a greater volume for the fluid to occupy thereby reducing the tendency of the fluid to accelerate.

As further support to the discussion on model convergence above, we provide an estimate of the rate of spatial convergence by employing Richardson extrapolation to estimate the exact values of the peak to peak variation in the three primary variables D, δ and u at a forcing frequency of $\omega = 1$. These estimated values of the primary variables are used to determine the error at three grid sizes $\Delta x = 0.011$ corresponding to $n = 146$ nodes, $\Delta x = 0.0054$ corresponding to $n = 291$ nodes and $\Delta x = 0027$ corresponding to $n = 581$ nodes and the results are shown in Figure 12. The linear relationship between error and the number of nodes on the log-log plot illustrates quadratic convergence with n as expected with the finite difference algorithms used in the model.

CONCLUSIONS

A one dimensional model of a paper forming process on a single wire crescent former was derived from fundamental conservation laws. The model is capable of describing both dynamic and steady-state behavior of the forming process. Examination of predicted steady-state geometry reveals that the pressure profile, drainage velocity and forming length are represented with reasonable accuracy when compared to test data. Once the parameter b (12) is calibrated using test data, predictions can be made of the steady-state that results from modest changes in the key

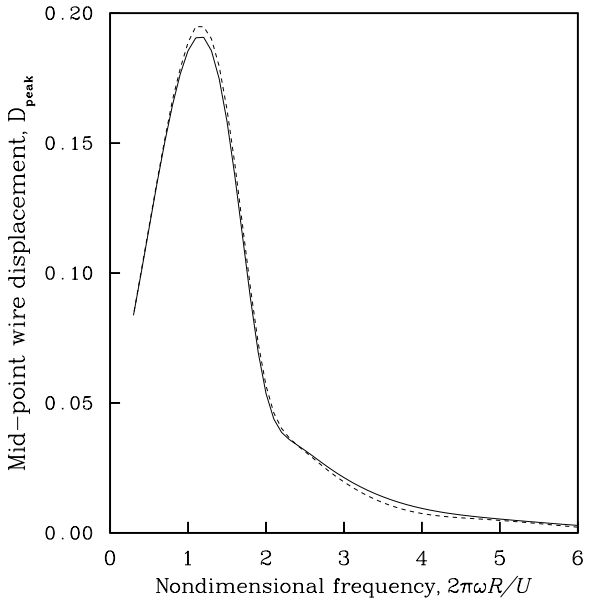

Figure 8: Frequency response of the wire at the midpoint ($x = L/2$). The peak-to-peak amplitude of the stable limit cycle ($D_{peak} = (D_{max} - D_{ss})/D_{ss}$) is shown as a function of frequency for a jet velocity disturbance amplitude of 2% of the steady-state jet velocity for $n = 291$ nodes ——— and $n = 146$ nodes - - - -.

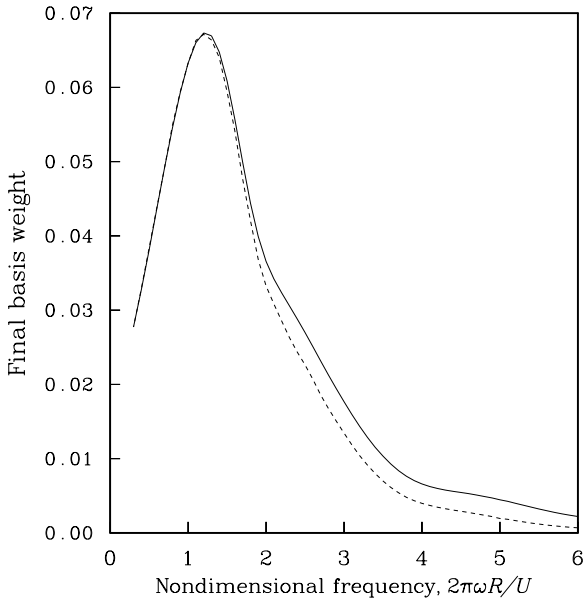

Figure 9: Frequency response of the basis weight of the mat leaving the forming region at $x = L$. The peak-to-peak amplitude of the stable limit cycle ($\delta_{peak} = (\delta_{max} - \delta_{ss})/\delta_{ss}$) is shown as a function of frequency for a jet velocity disturbance amplitude of 2% of the steady-state jet velocity for $n = 291$ nodes ——— and $n = 146$ nodes - - - -.

process parameters such as tension, machine speed, headbox consistency and the permeability characteristics of the mat and wire. Thus, the steady-state results help understand how these process parameters control the forming process in the absence of disturbances.

The free response of the model to an initial disturbance illustrates a large damping mechanism caused by the flow through the mat and wire. Computed frequency responses demonstrate that only the first system mode is excited and that higher modes of vibration are suppressed. Thus, the system effectively behaves as if it were a single degree of freedom system. Yet, despite the heavy damping, the model shows significant amplification of disturbances near resonant frequencies. The model predicts that 2% disturbances in jet velocity may result in nearly 7% variation in the basis weight as a result of the aforementioned resonance of the fundamental mode. Moreover, the resulting wavelength of these basis weight fluctuations are on the order of the roll radius. An experimental study by Perrault [5] shows large amplifications MD basis-weight variations at particular frequencies, but no direct comparisons can be made to the analysis because the process parameters are inadequately described.

Our latest work relaxes two assumptions made herein by including the effects of viscosity and variations in the cross-machine direction. The preliminary results indicate that the system solution remains remarkably similar to the one-dimensional inviscid model described here except in a very small region near the nip. The addition of viscosity appears to allow integration within a purely fluid computational domain nearly all the way to the nip without the requirement of a structure-dominated model nor a blending function.

ACKNOWLEDGMENTS

The authors thank E-June Chen (Univ. Michigan) and Dr. Jay Shands (Beloit Corp.) for useful discussions on this work. We also wish to acknowledge the Kimberly-Clark Corporation and the TAPPI Foundation for partial support of this study.

References

[1] Miller, G. F., *Proc. Royal Soc. London*, "Fluid Dynamics in a Papermaking Machine," **242**: 1-15 (1957).

[2] Schoeffler, J. D., *TAPPI Proc.*, "A Model of Sheet Formation and Drainage on Fourdrinier," **49**: 248-254 (1966).

[3] Baines, W. D., *Report to Pulp and Paper Research Institute of Canada*, "Flow in the Formation Region of a Two-Wire Machine," (1970).

[4] Turnbull, P. F., *Analysis of a Paper Forming Process.* PhD. Dissertation, U. Michigan. (1995).

[5] Perrault, J., *TAPPI J.*, "The influence of wet-end vibrations on machine-direction basis-weight variations," pp. 62-65 (1984).

[6] Mote, C. D. Jr., *Shock and Vib. Digest*, "Dynamic Stability of Axially Moving Materials," **4**: 2-11 (1972).

[7] Wickert, J. A. and Mote, C. D. Jr., *Shock and Vib. Digest*, "Current Research on the Vibration and Stability of Axially Moving Materials," **20**: 3-13 (1988).

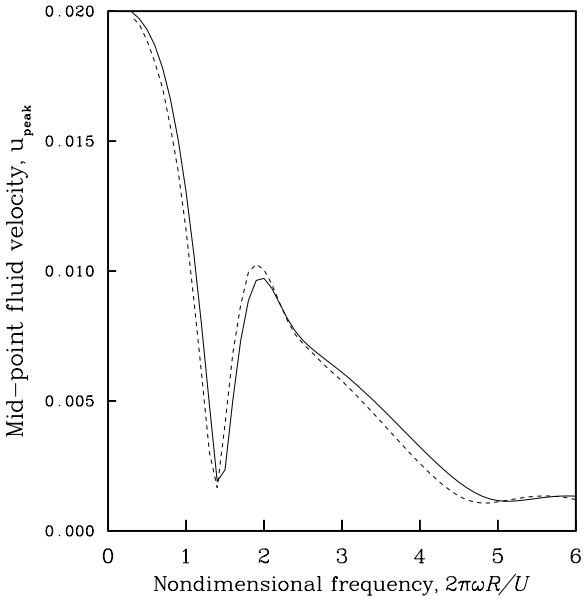

Figure 10: The frequency response of the fluid velocity $u_{peak}(x = L/2) = (u_{max} - u_{ss})/u_{ss}$ for a jet velocity disturbance amplitude of 2% of the steady-state jet velocity for $n = 291$ nodes ——— and $n = 146$ nodes - - - -.

[8] Yue, M. G., *ASME 6th Int. Power Transmission and Gearing Conference*, "Belt Vibration Considering Moving Contact and Parametric Excitation," **43**(1): 311-318, (1992).

[9] Turnbull, P. F., Perkins, N. C. and Schultz, W. W., *J. Vib. and Control*, "Contact Induced Nonlinearity in Oscillating Belts and Webs," **1**: 459-479 (1995).

[10] Pramila, A., *J. Sound and Vib.*, "Natural Frequencies of Submerged Axially Moving Band," **113**: 198-203 (1987).

[11] Chang, Y. B. and Moretti, P. M., *Proc. 1990 TAPPI Engineering Conference*, "Interaction of Fluttering Webs with Surrounding Air," 175-182 (1990).

[12] Lighthill, M. J., *J. Fluid Mech.*, "Notes on the Swimming of Slender Fish," **9**: 305-317 (1960).

[13] Kaviany, M., *Principles of Heat Transfer in Porous Media*, Springer-Verlag, pp. 62-64 (1991).

[14] Bhat, R. B., Xistris, G. D. and Sankar, T. S., *ASME J. Mech. Design*, "Dynamic Behavior of a Moving Belt Supported on Elastic Foundation," **104**: 143-147 (1982).

[15] Perkins, N. C., *ASME J. Vib. and Acoust.*, "Linear Dynamics of a Translating String on an Elastic Foundation," **112**: 2-7 (1990).

[16] Tan, C. A. and Zhang, J., *ASME J. Vib. and Acoust.*, "Dynamic Characteristics of a Constrained String Translating Across an Elastic Foundation," **116**: 318-325 (1994).

[17] Peyret, R. and Taylor, T. D., *Computational Methods for Fluid Flow*, Springer-Verlag, pp. 3-77 (1990).

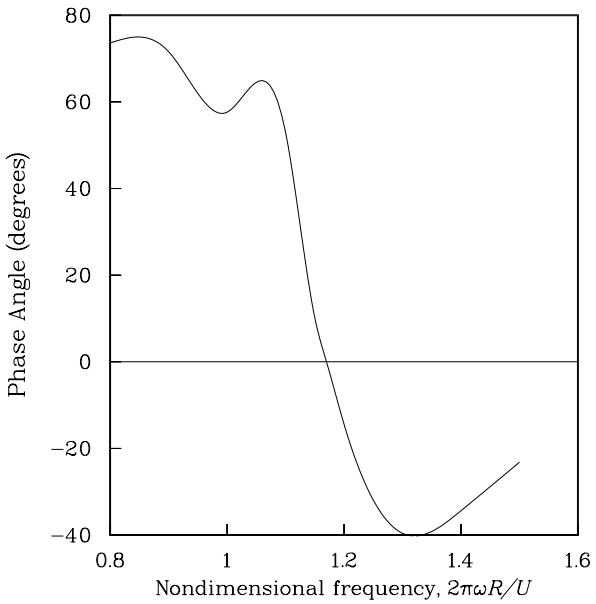

Figure 11: The phase difference between peaks in the wire displacement D and the fluid velocity u.

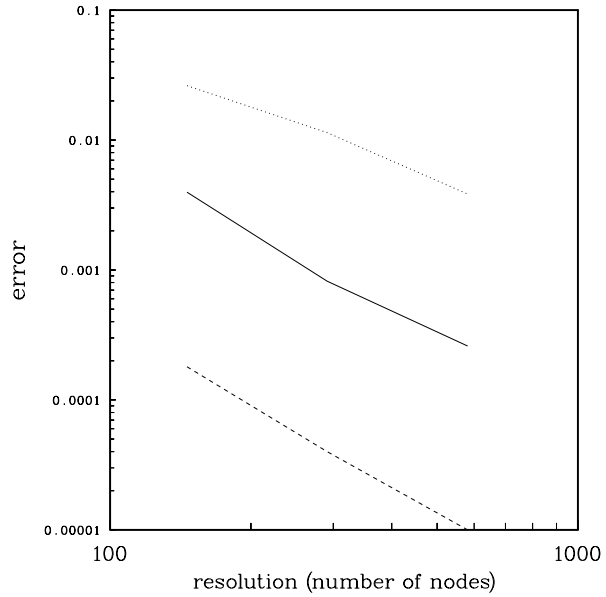

Figure 12: Quadratic spatial convergence of the three primary variables: $D =$ ———, $\delta =$ - - - -, and $u =$ ·····.